THE JOURNAL OF PHYSICAL CHEMISTRY Letters

Letter

pubs.acs.org/JPCL

Cesium Lead Halide Perovskites with Improved Stability for Tandem Solar Cells

Rachel E. Beal, Daniel J. Slotcavage, Tomas Leijtens, Andrea R. Bowring, Rebecca A. Belisle, William H. Nguyen, George F. Burkhard, Eric T. Hoke, and Michael D. McGehee*

Stanford University, Moore Materials Research Laboratory, 466 Lomita Mall, Palo Alto, California 94305, United States

Supporting Information

ABSTRACT: A semiconductor that can be processed on a large scale with a bandgap around 1.8 eV could enable the manufacture of highly efficient low cost double-junction solar cells on crystalline Si. Solution-processable organic−inorganic halide perovskites have recently generated considerable excitement as absorbers in single-junction solar cells, and though it is possible to tune the bandgap of $(CH_3NH_3)Pb(Br_xI_{1-x})_3$ between 2.3 and 1.6 eV by controlling the halide concentration, optical instability due to photoinduced phase segregation limits the voltage that can be extracted from compositions with appropriate bandgaps for tandem applications. Moreover, these materials have been shown to suffer from thermal degradation at temperatures within the processing and operational window. By replacing the volatile methylammonium cation with cesium, it is possible to synthesize a mixed halide absorber material with improved optical and thermal stability, a stabilized photoconversion efficiency of 6.5%, and a bandgap of 1.9 eV.

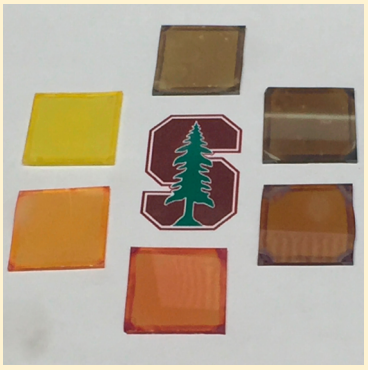

Tandem solar cells offer a promising avenue for increasing the efficiency of existing solar cell technologies with a minimal cost increase.[1−12] Viable top cell materials for use with an Si bottom cell should have an optical bandgap of ∼1.8 eV in order to achieve the maximum efficiency within the Shockley−Quiesser limit and be deposited via simple, scalable, low-temperature processing routes.[4] Organic−inorganic hybrid perovskites are generating considerable excitement as absorber materials in single-junction cells. Device efficiencies above 15% have been achieved through a variety of processing routes,[13−16] with a record power conversion efficiency of over 20% for an $(FA)PbI_3/(MA)PbBr_3$ (MA = CH_3NH_3, FA = $HC(NH_2)_2$) mixture.[16,17] To be impactful, perovskite absorber materials must display long-term stability at 85 °C, the upper end of the operational temperature range, and should ideally be stable at 150 °C, a typical curing temperature for ethylene-vinyl acetate (EVA) and many other commercial encapsulants. $(MA)PbX_3$ compounds have been shown to degrade at 85 °C due to the volatility of the organic MA cation,[18] motivating the investigation of $CsPbX_3$ materials because the inorganic Cs cation is much less volatile. Solar cells with $CsPbI_3$ and $CsPbBr_3$ absorber layers have recently been demonstrated.[19,20] $CsPbBr_3$ is an orthorhombic perovskite at room temperature with a bandgap of 2.25 eV.[21] The best reported device is stable in air and has a photoconversion efficiency (PCE) of 5.95%, V_{oc} of 1.28 V, and J_{sc} of 6.24 mA/cm^2 and is stable in air.[19] $CsPbI_3$ in the cubic perovskite phase has a more desirable bandgap of 1.73 eV, but the material transitions to a yellow, insulating, nonperovksite phase—also called the δ-phase—at temperatures below 315 °C.[20,22,23] Partial substitution of the relatively smaller Br for the bulky I anion should stabilize the structure and enable the synthesis of $CsPb(Br_xI_{1-x})_3$ perovskites that are thermodynamically favorable at room temperature.[24]

Controlling the halide stoichiometry in $(MA)PbX_3$ perovskites has been explored as a means of tuning the bandgap, but an optical instability where the peak photoluminescence red-shifts due to the perovskite separating into iodine-rich and bromine-rich phases under continued illumination reduces the voltage extracted and renders these materials ineffective as photovoltaic absorbers.[25−27] Here, we investigate $CsPb(Br_xI_{1-x})_3$ materials with x ranging from 0 to 1 and find that films with low Br concentrations maintain uniform halide composition under illumination. By substituting the $CsPbI_3$ lattice with 33% Br and annealing well below the transition temperature of 315 °C for the polycrystalline bulk material,[28] we are able to solution-process a 1.9 eV bandgap material with improved optical and thermal stability relative to MA-based perovskites and improved structural phase stability relative to $CsPbI_3$. Devices using this material have thus far yielded a stabilized PCE of 6.5%.

A series of films with increasing bromide fraction were spun from 0.4 M solutions of $CsPbI_3$ and $CsPbBr_3$ in dimethyl sulfoxide (DMSO) mixed in the appropriate molar ratio for the desired $CsPb(Br_xI_{1-x})_3$ composition. The exact composition of the x = 0.33 material used in devices was verified via ion chromatography on redissolved films. The measured I and Br fractions were 37.39% and 11.79% of the total mass, which corresponds to an I:Br ratio of 2.00:1 as expected. We have no reason to believe any iodine or bromine left any of the films we

Received: January 2, 2016
Accepted: February 10, 2016

DOI: 10.1021/acs.jpclett.6b00002
J. Phys. Chem. Lett. 2016, 7, 746−751

prepared and determined the composition of the other films based on the measured amounts of precursors that were put into the spin-casting solution.

The structure of all films was examined via X-ray diffraction, and all relevant XRD spectra are shown below in Figure 1. Note

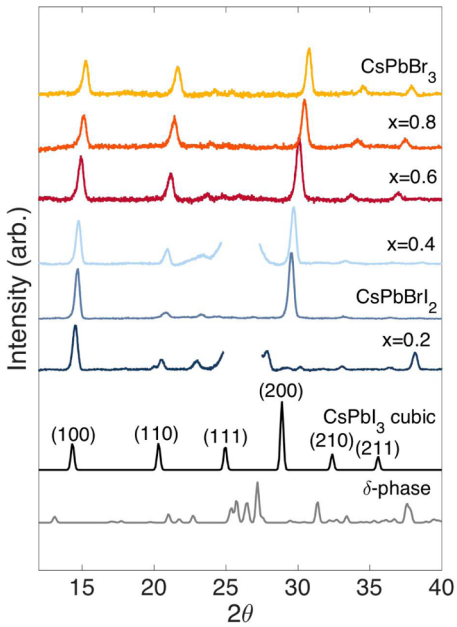

Figure 1. XRD spectra for $CsPb(Br_xI_{1-x})_3$, where x = 0 to 1. The spectrum of the membrane is introduces a large amorphous feature into the x = 0.2 and 0.4 spectra that is difficult to subtract cleanly and is cut off here for ease of viewing. The full spectra for x = 0.2, 0.4, and the membrane are included in the Supporting Information.

that the film of phase-pure $CsPbI_3$ transformed upon removal from the dry-air box, so the spectra shown here is from published first-principles calculations for the cubic perovskite $CsPbI_3$ structure.[29] A Mylar Chemplex Spectromembrane was used to protect the x = 0.4 and x = 0.2 samples resulting in a large amorphous feature centered around 2θ = 26° in both scans. The measured spectrum for $CsPbBr_3$ shown here is in good agreement with literature data for the orthorhombic perovskite structure, the notable difference between the cubic and orthorhombic spectra being the absence of a distinct (111) peak.[30] We note that the (100) and (200) peaks have increased relative intensity compared to literature data, suggesting that the processing route used here yields films that are somewhat oriented in the (100) direction. Because I is larger than Br, there should be a lattice contraction when Br substitutes for I. Thus, according to Bragg's law $n\lambda = 2d \sin\theta$, there should also be a corresponding shift in XRD peaks to higher angles as Br concentration increases. The XRD spectra for x = 0.8 and 0.6 are thus consistent with an orthorhombic perovskite lattice that is slightly dilated relative to $CsPbBr_3$. The relative intensity of the (110), (210), and (211) peaks are even further reduced in the spectra for the x = 0.4 and x = 0.33 compositions suggesting that these films are both oriented and in better agreement with a cubic rather than orthorhombic perovskite structure. In the scan for the x = 0.2 material, only the (100) and (110) perovskite peaks are present. No higher-angle perovskite peaks can be distinguished, and the peak at 2θ = 37° can be attributed to the delta phase. Although the perovskite peaks are dominant at low angles, the δ-phase peaks are more dominant at higher angles that were measured later in time, indicating that the material transitioned from the pseudocubic perovskite structure to the δ-phase over the course of the measurement. A spectrum for the room-temperature $CsPbI_3$ δ-phase from Stoumpos et al. is included for reference.[22]

The pseudocubic lattice parameter was also extracted from the (100) peak near 2θ = 15°. There is a lattice contraction with increasing Br content (Figure 2a) confirming that substitution on the anion site in $CsPbX_3$ is occurring. The absorption spectra in Figure 2b show that the bandgap increases with bromide fraction from about 1.77 to 2.38 eV.

Work by Hoke et al. has shown that $(MA)Pb(Br_xI_{1-x})_3$ compounds demonstrate a rapid redshift in photoluminescence wavelength due to photoinduced phase segregation for bromide concentrations exceeding 20% at fluences as low as 15 mW/cm^2, so we monitored the photoluminescence of the cesium mixed-halide perovskites to determine whether the same effect was present.[25] Figure 3 plots the peak photoluminescence wavelength for the same series of compositions over time. The PL peak position was stable over time for $CsPb(Br_xI_{1-x})_3$ films with $x \leq 0.4$ excited at a fluence of 100 mW/cm^2, equivalent to ~1 sun solar irradiation. The peak position for compositions with $0.4 < x < 1$, however, shifted significantly at the same excitation fluence. We speculate that the photoinduced phase separation involves the formation of iodine-rich and bromine-rich phases and that it occurs because the free energy of the semiconductor in the excited state can be reduced when the

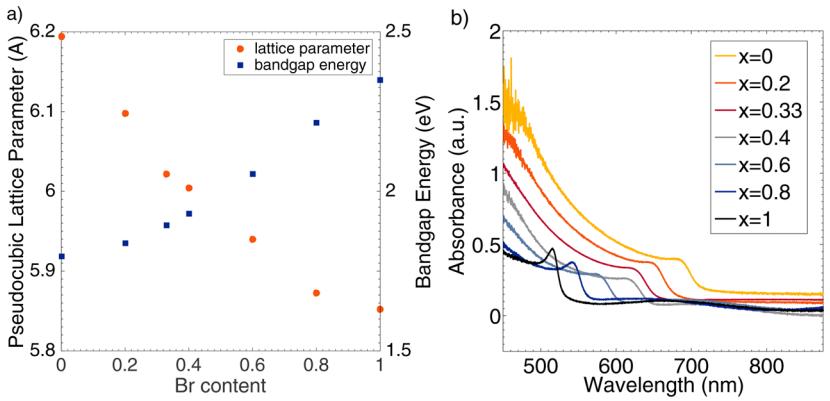

Figure 2. Change in (a) lattice parameter based on the shift in the (100) peak and concurrent change in the bandgap energy and (b) absorption onset in $CsPb(Br_xI_{1-x})_3$ with increasing Br content.

DOI: 10.1021/acs.jpclett.6b00002
J. Phys. Chem. Lett. 2016, 7, 746−751

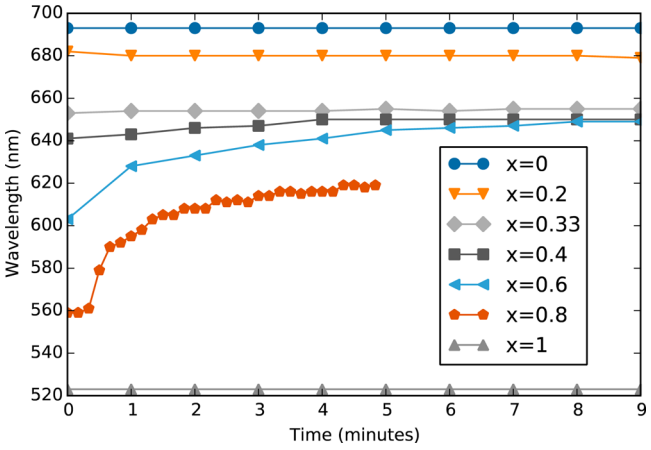

Figure 3. Photoluminescence peak position as a function of time for $CsPb(Br_xI_{1-x})_3$ materials under ~1 sun illumination.

charge carriers are able to migrate to the low bandgap phase. Although a full understanding of photoinduced phase separation in mixed halide perovskites is beyond the scope of this initial study, it is helpful to know that there is a broader range of stable compounds when cesium is used instead of methylammonium.

In the $CsPb(Br_xI_{1-x})_3$ family, the compounds with $0.2 < x < 0.4$ are most attractive for solar cells. When x is <0.2, the insulating δ phase is thermodynamically preferred at room temperature. When x is >0.4, phase separation occurs under illumination. $CsPbBrI_2$ with its bandgap around 1.9 eV was thus selected as a target composition for a solar cell absorber material.[24]

To further test the stability of $CsPbBrI_2$ against phase separation, a film was exposed to 100 mW/cm^2 for 1 h (Figure S2b). After its photoluminescence peak showed no significant shift in wavelength, the film was irradiated with a laser fluence of 1 W/cm^2. At 1 W/cm^2, the photoluminescence peak wavelength remained stable over the course of 10 min (Figure S3b). For both illumination intensities, though the photoluminescence peak position remained stable, the photoluminescence intensity dropped by almost an order of magnitude. Though the existence of this effect for $(MA)PbI_3$ is well known, its origins in both Cs and MA-based absorbers requires further investigation.[31]

The thermal stability of $CsPbBrI_2$ was also examined at 200 °C in an inert atmosphere, slightly higher than the typical curing temperature of ethylene-vinyl acetate (EVA) and other viable encapsulants.[32] The full absorption spectra were monitored over time via UV−vis spectroscopy. The $(MA)PbI_3$ control rapidly decomposed to PbI_2 after just 10 min at only 180 °C as indicated by the absorption edge shifting from 780 to around 520 nm.[18,33] The absorption onset in $CsPbBrI_2$ is comparatively stable even at the higher temperature (Figure 4). Future work will examine the thermal stability of optimized films to better assess long-term thermal stability.

Solar cells using $CsPbBrI_2$ in an inverted architecture were prepared using the architecture in Figure S4a. A 150 nm-thick perovskite layer was spun on a poly(3,4-ethylenedioxythiophene) polystyrenesulfonate (PEDOT:PSS) hole transport layer on an indium tin oxide (ITO)-coated glass substrate. [6,6]-phenyl-C61 butyric acid methyl ester ([60]PCBM) was used as a hole transport layer with 8 nm of [2,9]-dimethy-[4,7]-diphenyl-[1,10]-phenanthroline (BCP) as a hole-blocking layer and 100 nm of Al as an electron selective contact. The as-spun perovskite layer was preannealed at 65 °C for 5 min to form the cubic perovskite phase and then immediately annealed at 135 °C for an additional 15 min to drive off solvent. As shown in Figure 5b, cells had a champion PCE of 6.69% when scanned from positive to negative voltage and 6.80% when scanned from negative to positive voltage with a V_{oc} of 1.12 and 1.06 V, respectively, and a J_{sc} of 10.9 mA/cm^2 in both cases. Maximum power point tracking gave a stabilized efficiency of 6.5% (Figure 5a). The external quantum efficiency of the device (Figure 5c) shows a maximum in absorption around 500 nm and a reduction in EQE at shorter wavelengths that can likely be attributed to parasitic absorption in the ITO.

With a bandgap of approximately 1.9 eV, $CsPbBrI_2$ could have a J_{sc} as high as 17.1 mA/cm^2 under the AM 1.5G spectrum. It should be possible to significantly improve device efficiency with better materials processing. The perovskite absorber layer is very thin, ~ 150 nm, with some pinholes that can be seen in an SEM image (Figure S4b), so shunts in the device is likely to reduce the fill factor and V_{oc}, whereas J_{sc} is likely limited by absorption. Thicker films could not be prepared via the one-step deposition of stoichiometric solutions because solution concentration was limited to 0.4 M by the solubility limit of CsBr. Work on developing a processing route that yields thicker films with better morphology is ongoing, and

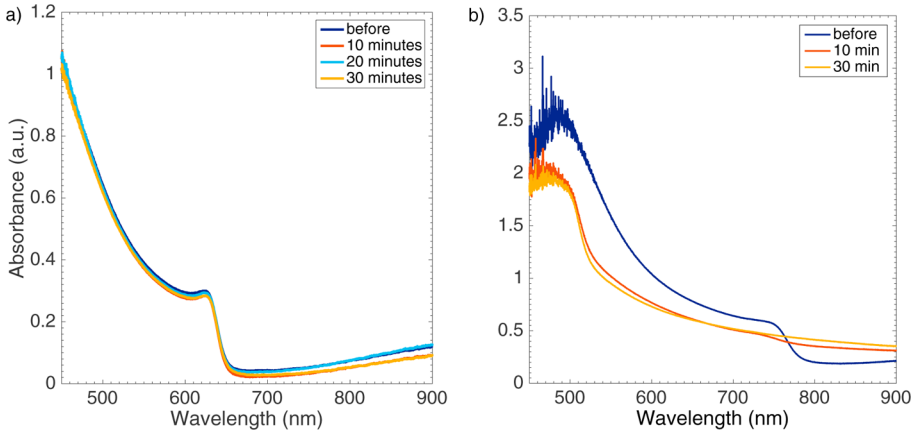

Figure 4. Absorption spectra for (a) $CsPbBrI_2$ and (b) $(MA)PbI_3$ after heating at 180 °C showing that the absorption onset for $CsPbBrI_2$ is stable on a time scale where the optical properties of $(MA)PbI_3$ degrade.

DOI: 10.1021/acs.jpclett.6b00002
J. Phys. Chem. Lett. 2016, 7, 746−751

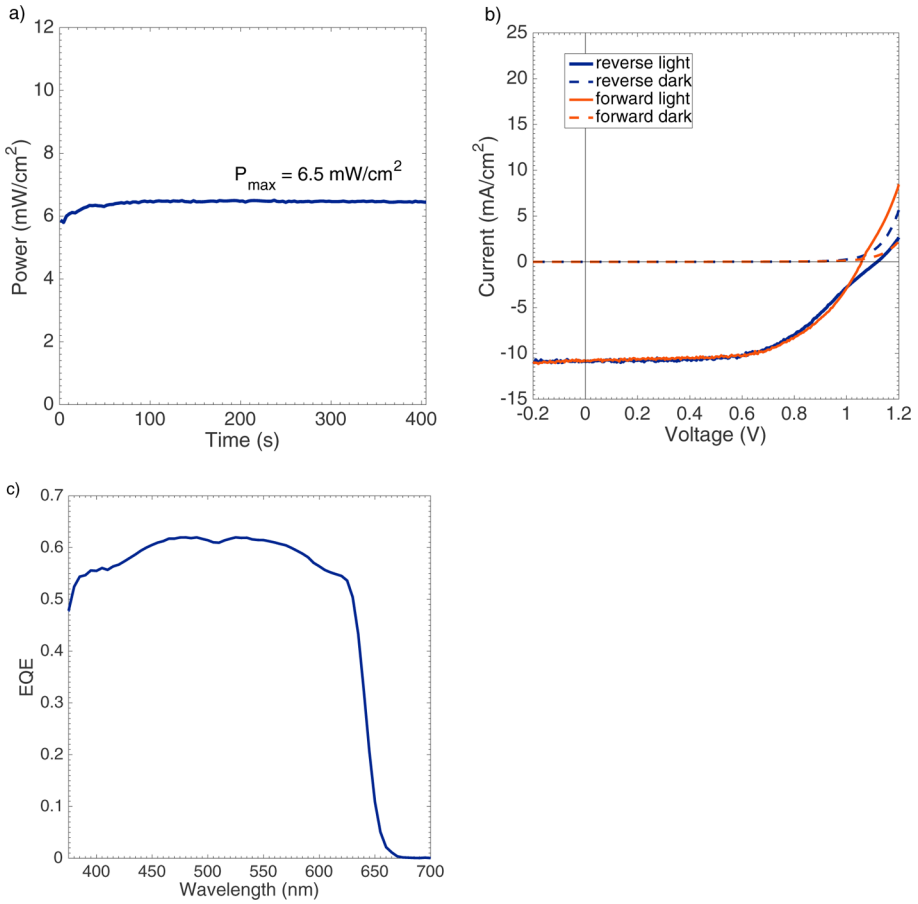

Figure 5. (a) Stabilized power output and (b) current density−voltage characteristics (0.025 V/s scan rate) for the champion device; (c) external quantum efficiency for a representative device with an integrated current of 9.5 mA/cm^2 (see Figure S5 for steady-state J_{sc}).

an optimized perovskite layer should yield a cell with significantly improved performance in all parameters. Further investigation of the energy levels in the material will enable better contact selection to maximize V_{oc} and photoconversion efficiency. Recent reports of the successful fabrication of single junction devices with Cs-stabilized FA-based perovskite absorbers suggest that further bandgap tuning may also be possible via the substitution of (MA) or (FA) on the cation site.[34−38] With further optimization, the future of Cs-based mixed-halide perovskites as potential absorbers in tandem top-cells and other optoelectronic applications such as LEDs is bright.

EXPERIMENTAL METHODS

Materials Synthesis and Characterization. For all films and devices, 0.4 M solutions of $CsPbBr_3$ and $CsPbI_3$ in dimethyl sulfoxide (DMSO) were prepared using CsBr, CsI, $PbBr_2$, PbI_2 precursors and mixed in the appropriate molar ratios for the $CsPb(Br_xI_{1-x})_3$ target composition. Solutions were prepared under an inert atmosphere in an N_2 glovebox with <5 ppm of O_2 and H_2O, dissolved at 150 °C for 1 h, filtered through a 200 nm PTFE filter, and then transferred to a dry-air box for deposition processes. Films for XRD, absorption, photoluminescence, and thermal stability measurements were prepared by spinning 80 μL of solution at 2000 rpm for 60 s. The glass substrates were cleaned, UV-ozone treated for 30 min, and heated to 65 °C along with the filtered solutions in the dry-air box for at least 15 min prior to deposition, which was done rapidly while the substrate and solution were still at an elevated temperature. Films with $x \geq 0.4$ were annealed at 65 °C for 1 h, but films with $x \leq 0.2$ were found to change color from brown-black to yellow, presumably transitioning to the more thermodynamically stable δ-phase, over the course of such a long annealing time. These films were heated for only 15 min and characterized immediately after the annealing step. Films for photoluminescence and XRD measurements were also capped with a 50 mg/mL polystyrene solution in chlorobenzene spun at 2000 rpm for 30 s.

X-ray diffraction spectra were measured on a Panalytical X'Pert Pro Diffractometer (Copper anode, $K\alpha_1$ = 1.54060 Å, $K\alpha_2$ = 1.54443 Å, $K\alpha_2/K\alpha_1$ ratio = 0.50). A Mylar Chemplex Spectromembrane was used to protect air sensitive samples during XRD characterization. All other characterization and device testing was done in a dry N_2 box unless otherwise specified. Absorption was measured with an Ocean Optics USB4000 photospectrometer and an HL-200 halogen light source using a blank glass slide as a reference sample. In thermal stability tests, $CsPbBrI_2$ samples were heated in a dry N_2 box (O_2 < 15 ppm) at either 85 or 180 °C alongside $(MA)PbI_3$ control samples prepared via a spectator-ion method with lead acetate that has been used to produce our lab's highest-efficiency MA-based devices,[39] and absorption was measured as a function time. Photoluminescence measurements were performed with a 488 nm CW laser at 100 mW/cm^2 (unless otherwise specified) for $CsPb(Br_xI_{1-x})_3$ with $0 \leq x \leq 0.6$ and 375 nm CW laser at 130 mW/cm^2 for $0.8 \leq x \leq 1$. PL samples were kept in an N_2 chamber during measurement.

DOI: 10.1021/acs.jpclett.6b00002
J. Phys. Chem. Lett. 2016, 7, 746−751

Device Fabrication and Testing. For devices, 10 Ω/square ITO substrates were again cleaned and UV-ozone treated for 30 min, then coated with a ∼ 30 nm thick PEDOT:PSS hole transport layer (Figure S4b) spun at 4000 rpm for 30 s in ambient conditions. Substrates and films were heated and deposited as above. After spinning, the coated substrates were heated for 5 min at 65 °C so that a uniform brownish black perovskite layer with little optical haze formed and were then annealed for an additional 15 min at 135 °C. The unfinished devices were then allowed to cool to room temperature before the deposition of the electron transport layer. 80 μL of 22 wt % [6,6]-phenyl-C_{61}-butyric acid methyl ester ([60]PCBM) was pipetted onto the perovskite layer and spun at 3000 rpm for 40 s. The [60]PCBM layer was annealed for 7 min at 85 °C, and the unfinished devices were left overnight in a dry N_2 glovebox. Then, 8 nm of bathocuproine (BCP) and 100 nm of Al (Figure S4b) were evaporated as a hole-blocking layer and an electron selective contact, respectively. *J*−*V* curves were measured using a Keithley 2400 source meter and a SpectraPhysics 91160-1000 solar simulator calibrated to one sun AM1.5 G using a NREL certified KG-5 filtered silicon photodiode. The external quantum efficiency (EQE) was recorded as a function of the wavelength using a Keithley model 236 without light bias. A 100 W tungsten lamp (Newport) was used to provide an excitation beam, which was focused through a Princeton Instruments SpectraPro 150 monochromator and chopped at approximately 1 Hz. At each wavelength, data was collected for and averaged for 5s.

■ ASSOCIATED CONTENT

Supporting Information

The Supporting Information is available free of charge on the ACS Publications website at DOI: 10.1021/acs.jpclett.6b00002.

Experimental, materials, and device fabrication details are included in addition to additional photoluminescence spectra. (PDF)

■ AUTHOR INFORMATION

Corresponding Author

* E-mail: mmcgehee@stanford.edu.

Notes

The authors declare no competing financial interest.

■ ACKNOWLEDGMENTS

R.E.B. acknowledges government support by the Department of Defense through the National Defense Science and Engineering Graduate Fellowship (NDSEG) Program. D.J.S. and A.R.B. acknowledge support from Stanford University through Benchmark Stanford Graduate Fellowships. A.R.B also acknowledges support from the National Science Foundation Graduate Research Fellowship Program under Grant No. 1147470. All authors acknowledge support from the Department of Energy through the Bay Area Photovoltaic Consortium under Award Number DE-EE0004946 and through the Sunshot NextGen III program under Award Number DE-EE0006707.

■ REFERENCES

(1) Bailie, C. D.; Christoforo, M. G.; Mailoa, J. P.; Bowring, A. R.; Unger, E. L.; Nguyen, W. H.; Burschka, J.; Pellet, N.; Lee, J. Z.; Grätzel, M.; et al. Polycrystalline Tandem Photovoltaics Using Perovskites on Top of Silicon and CIGS. *Energy Environ. Sci.* **2014**, *8*, 956−963.

(2) Todorov, T.; Gershon, T.; Gunawan, O.; Sturdevant, C.; Guha, S. Perovskite-Kesterite Monolithic Tandem Solar Cells with High Open-Circuit Voltage. *Appl. Phys. Lett.* **2014**, *105*, 173902.

(3) Löper, P.; Moon, S. J.; Martin de Nicolas, S.; Niesen, B.; Ledinsky, M.; Nicolay, S.; Bailat, J.; Yum, J. H.; De Wolf, S.; Ballif, C. Organic-Inorganic Halide Perovskite/crystalline Silicon Four-Terminal Tandem Solar Cells. *Phys. Chem. Chem. Phys.* **2015**, *17*, 1619−1629.

(4) Bailie, C. D.; McGehee, M. D. High-Efficiency Tandem Perovskite Solar Cells. *MRS Bull.* **2015**, *40*, 681−686.

(5) Kranz, L.; Abate, A.; Feurer, T.; Fu, F.; Avancini, E.; Löckinger, J.; Reinhard, P.; Zakeeruddin, S. M.; Grätzel, M.; Buecheler, S.; et al. High-Efficiency Polycrystalline Thin Film Tandem Solar Cells. *J. Phys. Chem. Lett.* **2015**, *6*, 2676−2681.

(6) Lang, F.; Gluba, M. A.; Albrecht, S.; Rappich, J.; Korte, L.; Rech, B.; Nickel, N. H. Perovskite Solar Cells with Large-Area CVD-Graphene for Tandem Solar Cells. *J. Phys. Chem. Lett.* **2015**, *6*, 2745−2750.

(7) Mailoa, J. P.; Bailie, C. D.; Johlin, E. C.; Hoke, E. T.; Akey, A. J.; Nguyen, W. H.; McGehee, M. D.; Buonassisi, T. A 2-Terminal Perovskite/silicon Multijunction Solar Cell Enabled by a Silicon Tunnel Junction. *Appl. Phys. Lett.* **2015**, *106*, 121105.

(8) Sheng, R.; Ho-Baillie, A. W.-Y.; Huang, S.; Keevers, M.; Hao, X.; Jiang, L.; Cheng, Y.-B.; Green, M. A. 4-Terminal Tandem Solar Cells Using $CH_3NH_3PbBr_3$ by Spectrum Splitting. *J. Phys. Chem. Lett.* **2015**, *6*, 3931−3934.

(9) Todorov, T.; Gershon, T.; Gunawan, O.; Lee, Y. S.; Sturdevant, C.; Chang, L.-Y.; Guha, S. Monolithic Perovskite-CIGS Tandem Solar Cells via In Situ Band Gap Engineering. *Adv. Energy Mater.* **2015**, *5*, 1500799.

(10) Uzu, H.; Ichikawa, M.; Hino, M.; Nakano, K.; Meguro, T.; Hernández, J. L.; Kim, H.-S.; Park, N.-G.; Yamamoto, K. High Efficiency Solar Cells Combining a Perovskite and a Silicon Heterojunction Solar Cells via an Optical Splitting System. *Appl. Phys. Lett.* **2015**, *106*, 013506.

(11) Werner, J.; Dubuis, G.; Walter, A.; Löper, P.; Moon, S.-J.; Nicolay, S.; Morales-Masis, M.; De Wolf, S.; Niesen, B.; Ballif, C. Sputtered Rear Electrode with Broadband Transparency for Perovskite Solar Cells. *Sol. Energy Mater. Sol. Cells* **2015**, *141*, 407−413.

(12) Yang, Y. M.; Chen, Q.; Hsieh, Y.-T.; Song, T.-B.; Marco, N.; Zhou, H.; Yang, Y. Multilayer Transparent Top Electrode for Solution Processed Perovskite/Cu(In,Ga) $(Se,S)_2$ Four Terminal Tandem Solar Cells. *ACS Nano* **2015**, *9*, 7714−7721.

(13) Kojima, A.; Teshima, K.; Shirai, Y.; Miyasaka, T. Organometal Halide Perovskites as Visible-Light Sensitizers for Photovoltaic Cells. *J. Am. Chem. Soc.* **2009**, *131*, 6050−6051.

(14) Zhou, H.; Chen, Q.; Li, G.; Luo, S.; Song, T. -b.; Duan, H.-S.; Hong, Z.; You, J.; Liu, Y.; Yang, Y. Interface Engineering of Highly Efficient Perovskite Solar Cells. *Science (Washington, DC, U. S.)* **2014**, *345*, 542−546.

(15) Jeon, N. J.; Noh, J. H.; Yang, W. S.; Kim, Y. C.; Ryu, S.; Seo, J.; Seok, S. Il. Compositional Engineering of Perovskite Materials for High-Performance Solar Cells. *Nature* **2015**, *517*, 476−480.

(16) Yang, W. S.; Noh, J. H.; Jeon, N. J.; Kim, Y. C.; Ryu, S.; Seo, J.; Seok, S. I. High-Performance Photovoltaic Perovskite Layers Fabricated through Intramolecular Exchange. *Science (Washington, DC, U. S.)* **2015**, *348*, 1234−1237.

(17) *NREL Efficiency Chart, Revision 06/08/2015*; U.S. Department of Energy, Office of Energy Efficiency and Renewable Energy: Washington, DC, 2015; http://www.nrel.gov/ncpv/images/efficiency_chart.jpg (accessed June 8, 2015).

(18) Conings, B.; Drijkoningen, J.; Gauquelin, N.; Babayigit, A.; D'Haen, J.; D'Olieslaeger, L.; Ethirajan, A.; Verbeeck, J.; Manca, J.; Mosconi, E.; et al. Intrinsic Thermal Instability of Methylammonium Lead Trihalide Perovskite. *Adv. Energy Mater.* **2015**, *5* (15), 1500477.

(19) Kulbak, M.; Cahen, D.; Hodes, G. How Important Is the Organic Part of the Lead Halide Perovskite Photovoltaic Cells? Efficient $CsPbBr_3$ Cells. *J. Phys. Chem. Lett.* **2015**, *6*, 2452.

DOI: 10.1021/acs.jpclett.6b00002
J. Phys. Chem. Lett. 2016, 7, 746−751

(20) Eperon, G. E.; Paternò, G. M.; Sutton, R. J.; Zampetti, A.; Haghighirad, A. A.; Cacialli, F.; Snaith, H. J. Inorganic Caesium Lead Iodide Perovskite Solar Cells. *J. Mater. Chem. A* **2015**, *3*, 19688.
(21) Stoumpos, C. C.; Malliakas, C. D.; Peters, J. a; Liu, Z.; Sebastian, M.; Im, J.; Chasapis, T. C.; Wibowo, A. C.; Chung, D. Y.; Freeman, A. J.; et al. Crystal Growth of the Perovskite Semiconductor $CsPbBr_3$: A New Material for High-Energy Radiation Detection. *Cryst. Growth Des.* **2013**, *13*, 2722−2727.
(22) Stoumpos, C. C.; Malliakas, C. D.; Kanatzidis, M. G. Semiconducting Tin and Lead Iodide Perovskites with Organic Cations: Phase Transitions, High Mobilities, and near-Infrared Photoluminescent Properties. *Inorg. Chem.* **2013**, *52*, 9019−9038.
(23) Akkerman, Q. A.; D'Innocenzo, V.; Accornero, S.; Scarpellini, A.; Petrozza, A.; Prato, M.; Manna, L. Tuning the Optical Properties of Cesium Lead Halide Perovskite Nanocrystals by Anion Exchange Reactions. *J. Am. Chem. Soc.* **2015**, *137*, 10276−10281.
(24) Yin, W. J.; Yan, Y.; Wei, S. H. Anomalous Alloy Properties in Mixed Halide Perovskites. *J. Phys. Chem. Lett.* **2014**, *5*, 3625−3631.
(25) Hoke, E. T.; Slotcavage, D. J.; Dohner, E. R.; Bowring, A. R.; Karunadasa, H. I.; McGehee, M. D. Reversible Photo-Induced Trap Formation in Mixed-Halide Hybrid Perovskites for Photovoltaics. *Chem. Sci.* **2015**, *6*, 613−617.
(26) Noh, J. H.; Im, S. H.; Heo, J. H.; Mandal, T. N.; Seok, S. Il. Chemical Management for Colorful, Efficient, and Stable Inorganic-Organic Hybrid Nanostructured Solar Cells. *Nano Lett.* **2013**, *13*, 1764−1769.
(27) Sadhanala, A.; Deschler, F.; Thomas, T. H.; Dutton, S. E.; Goedel, K. C.; Hanusch, F. C.; Lai, M. L.; Steiner, U.; Bein, T.; Docampo, P.; et al. Preparation of Single-Phase Films of $CH_3NH_3Pb(I_{1-x}Br_x)_3$ with Sharp Optical Band Edges. *J. Phys. Chem. Lett.* **2014**, *5*, 2501−2505.
(28) Protesescu, L.; Yakunin, S.; Bodnarchuk, M. I.; Krieg, F.; Caputo, R.; Hendon, C. H.; Yang, R. X.; Walsh, A.; Kovalenko, M. V. Nanocrystals of Cesium Lead Halide Perovskites ($CsPbX_3$, x = Cl, Br, and I): Novel Optoelectronic Materials Showing Bright Emission with Wide Color Gamut. *Nano Lett.* **2015**, *15*, 3692.
(29) Murtaza, G.; Ahmad, I. First Principle Study of the Structural and Optoelectronic Properties of Cubic Perovskites $CsPbM_3$ (M = Cl, Br, I). *Phys. B* **2011**, *406*, 3222−3229.
(30) Rodová, M.; Brožek, J.; Knížek, K.; Nitsch, K. Phase Transitions in Ternary Caesium Lead Bromide. *J. Therm. Anal. Calorim.* **2003**, *71*, 667−673.
(31) Gottesman, R.; Gouda, L.; Kalanoor, B. S.; Haltzi, E.; Tirosh, S.; Rosh-Hodesh, E.; Tischler, Y.; Zaban, A.; Quarti, C.; Mosconi, E.; et al. Photoinduced Reversible Structural Transformations in Free-Standing $CH_3NH_3PbI_3$ Perovskite Films. *J. Phys. Chem. Lett.* **2015**, *6*, 2332−2338.
(32) Mei, Z.; Pern, F. J.; Glick, S. H. *Modified EVA Encapsulant Formulations for Low Temperature Processing*; U.S. Department of Energy, Office of Energy Efficiency and Renewable Energy: Washington, DC, 2001.
(33) Deretzis, I.; Alberti, A.; Pellegrino, G.; Smecca, E.; Giannazzo, F.; Sakai, N.; Miyasaka, T.; La Magna, A. Atomistic Origins of $CH_3NH_3PbI_3$ Degradation to PbI2 in Vacuum. *Appl. Phys. Lett.* **2015**, *106*, 131904.
(34) Yi, C.; Luo, J.; Meloni, S.; Boziki, A.; Ashari-Astani, N.; Grätzel, C.; Zakeeruddin, S. M.; Rothlisberger, U.; Grätzel, M. Entropic Stabilization of Mixed A-Cation ABX_3 Metal Halide Perovskites for High Performance Perovskite Solar Cells. *Energy Environ. Sci.* **2016**, *9*, 656−662.
(35) Lee, J.-W.; Kim, D.-H.; Kim, H.-S.; Seo, S.-W.; Cho, S. M.; Park, N.-G. Formamidinium and Cesium Hybridization for Photo- and Moisture-Stable Perovskite Solar Cell. *Adv. Energy Mater.* **2015**, *5*, 1501310.
(36) McMeekin, D. P.; Sadoughi, G.; Rehman, W.; Eperon, G. E.; Saliba, M.; Horantner, M. T.; Haghighirad, A.; Sakai, N.; Korte, L.; Rech, B.; et al. A Mixed-Cation Lead Mixed-Halide Perovskite Absorber for Tandem Solar Cells. *Science (Washington, DC, U. S.)* **2016**, *351*, 151−155.
(37) Li, Z.; Yang, M.; Park, J.-S.; Wei, S.-H.; Berry, J.; Zhu, K. Stabilizing Perovskite Structures by Tuning Tolerance Factor: Formation of Formamidinium and Cesium Lead Iodide Solid-State Alloys. *Chem. Mater.* **2016**, *28*, 284.
(38) Choi, H.; Jeong, J.; Kim, H.-B.; Kim, S.; Walker, B.; Kim, G.-H.; Kim, J. Y. Cesium-Doped Methylammonium Lead Iodide Perovskite Light Absorber for Hybrid Solar Cells. *Nano Energy* **2014**, *7*, 80−85.
(39) Zhang, W.; Saliba, M.; Moore, D. T.; Pathak, S.; Horantner, M.; Stergiopoulos, T.; Stranks, S. D.; Eperon, G. E.; Alexander-Webber, J. a; Abate, A.; et al. Ultrasmooth Organic-Inorganic Perovskite Thin-Film Formation and Crystallization for Efficient Planar Heterojunction Solar Cells. *Nat. Commun.* **2015**, *6*, 6142.

DOI: 10.1021/acs.jpclett.6b00002
J. Phys. Chem. Lett. 2016, 7, 746−751